Coal-Derived Alternatives to Fiber-Cementitious Building Materials
Final Technical Report

DOE Cooperative Agreement No. DE-FE0031981

Project PI: Jason Trembly
Phone: (740) 566-7046
E-mail: trembly@ohio.edu

Project Period:
January 1, 2021 through December 31, 2022

Prepared by:

Yahya Al-Majali, Logan Veley, Mingcong Zhang, Rudolph Olson III, Eric Shereda, and Jason Trembly

Submitted by:

Ohio University
1 Ohio University
Athens, OH 45701

Submitted to:
U.S. Department of Energy
Office of Fossil Energy and Carbon Management
National Energy Technology Laboratory

Disclaimer

Acknowledgment

This material is based upon work supported by the Department of Energy National Energy Technology Laboratory under award Number DE-FE0031981.

Abstract

This report examines the development and use of coal-derived foam cladding materials for use in building applications. Foam materials were developed at bench scale and evaluated for cladding applications. Techno-economic analyses are also reported.

Table of Contents

1. Introduction

The primary goal of the National Energy Technology Laboratory's Carbon Ore Processing is to develop novel technologies for producing valuable products from coal and coal wastes. The objective of this project was to evaluate the development and application coal-derived alternatives to cementitious materials in building sector, with a specific focus on composite cladding applications.

1.1. Project Objectives

The objective of this project is to develop coal-based siding materials used in residential and commercial building cladding applications. Project objectives included conducting bench-scale coal extrusion trials to assess material properties and technical feasibility for siding and related applications, developing molecular dynamic simulations to predict properties of coal siding materials, identifying and analyzing existing siding market applications and related market applications for coal siding materials, and conducting techno-economic and technology gap analyses to identify required selling prices and resources necessary to scale up and commercialize coal siding materials.

2. Siding Development

2.1. Coal-derived carbon foam materials

2.1.1. Elemental Analysis

Elemental analysis for carbon foam materials was conducted using Flash 2000 CHNS-O analyzer to determine carbon, hydrogen, nitrogen, oxygen, and sulfur content. The analysis was conducted for several types of foam including as-extruded foam (green foam extruded at 450 °C) and five additional foams obtained from green foam by thermal treatments at different temperatures (700 °C, 800 °C, 900 °C,1000 °C, and 1100 °C). Results indicated carbon represents the major element, and as expected, carbon content increased with treatment temperature (Figure 1a). Hydrogen content substantially decreased (Figure 1b) due to the promotion of degree of aromatization, which resulted from the association or elimination of -OH, -CH3, -CH2, and -C=O groups in carbon foam [1]. Nitrogen content was not significantly different for the lower temperature foams (green, 700 °C, 800 °C), while inverse proportionality was evident for the higher temperature foams (Figure 1c). Sulfur content remained comparable for the different foams (Figure 1d), indicating most sulfur is part of a highly stable chemical structure (e.g., aromatic species). Similar to hydrogen, oxygen content dramatically dropped for the foam treated at 700 °C, while a second big drop was evident for foams treated at 1000 °C and 1100 °C (Figure 1e).

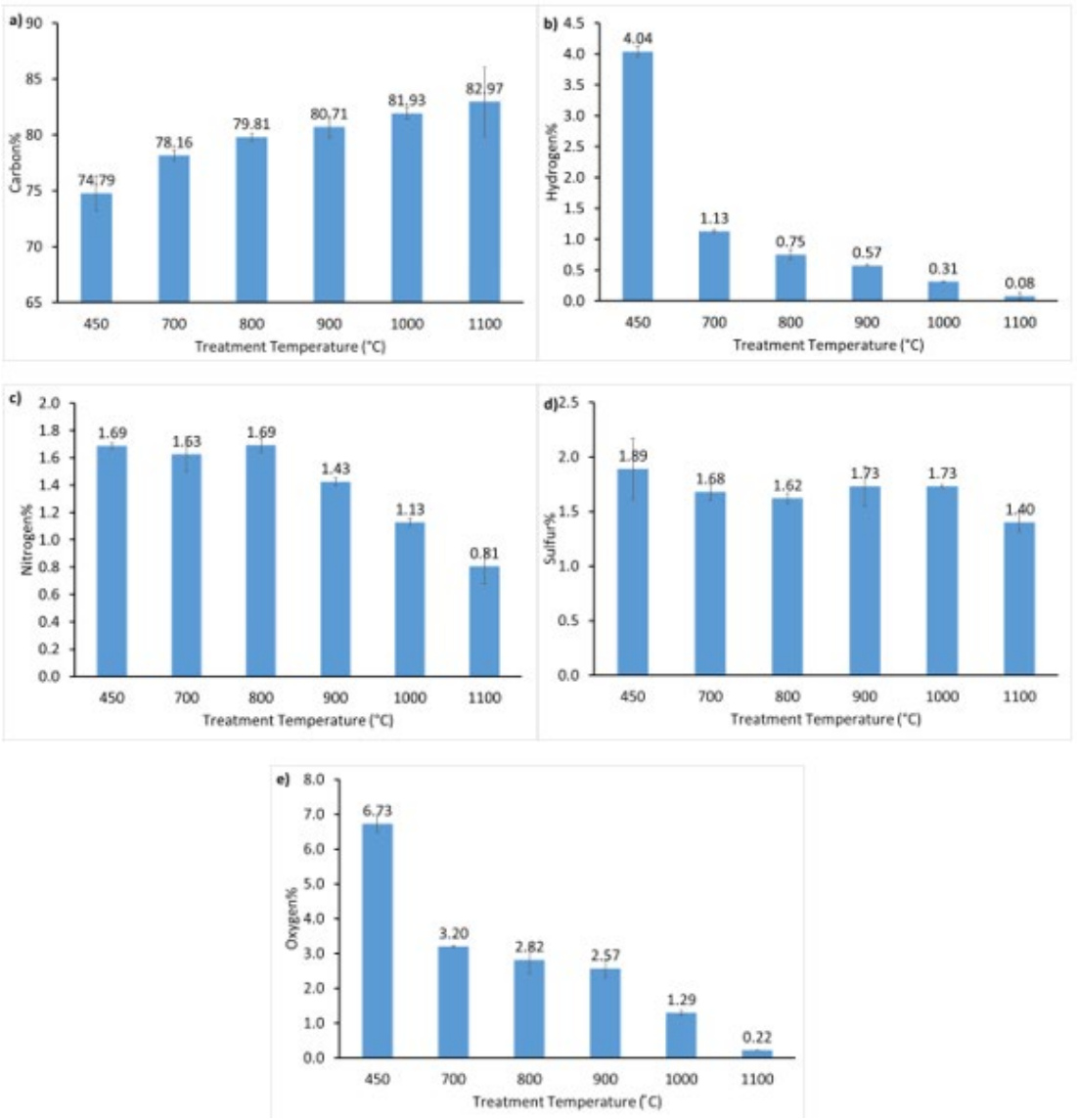

Figure 1: Ultimate analyses for carbon foam materials including green foam (450 °C) and foam treated at different temperatures (700 °C, 800 °C, 900 °C, 1000 °C, 1100 °C)

2.1.2. Thermogravimetric Analysis (TGA)

Thermo-oxidative stability for carbon foam was characterized using thermogravimetric analysis (TGA). Six types of carbon foam were investigated: one foam material being "green" in nature (extruded at 450 °C) and five additional foams obtained from green foam by thermal treatments at different temperatures (700 °C, 800 °C, 900 °C,1000 °C, and 1100 °C). Testing and thermal analysis were conducted in accordance with recommendations by International Confederation for Thermal Analysis and Calorimetry (ICTAC) [2], [3]. Powdered specimens (10 ± 0.5mg) were tested at four different heating rates (5 °C/min, 10 °C/min, 15 °C/min, 20 °C/min) under air atmosphere.

Figure 2 shows TGA and differential thermogravimetric (DTG) curves for the different foams. It can be seen that all foams, except green and 1100 °C foam, have a single-step degradation, and increasing treatment temperature (700 °C to 1100 °C) has shifted the degradation curve toward higher temperature

values, indicating higher thermal stability. For example, the temperature at maximum degradation rate (T_{max}) was shifted from 509 °C for the 700 °C foam to 769 °C for the 1100 °C foam. This shift was expected as the thermal treatment improve the chemical structure of the foam. In comparison to the rest of foam materials, a bigger shift in the degradation peak for the 1100 °C foam was noticed. As for the green and 1100 °C foams, the DTG curves suggest a multistep degradation, indicting a complicated degradation mechanism. For all treated foams, the degradation rate was decreased as treatment temperature increased which is also indicative of higher thermal stability.

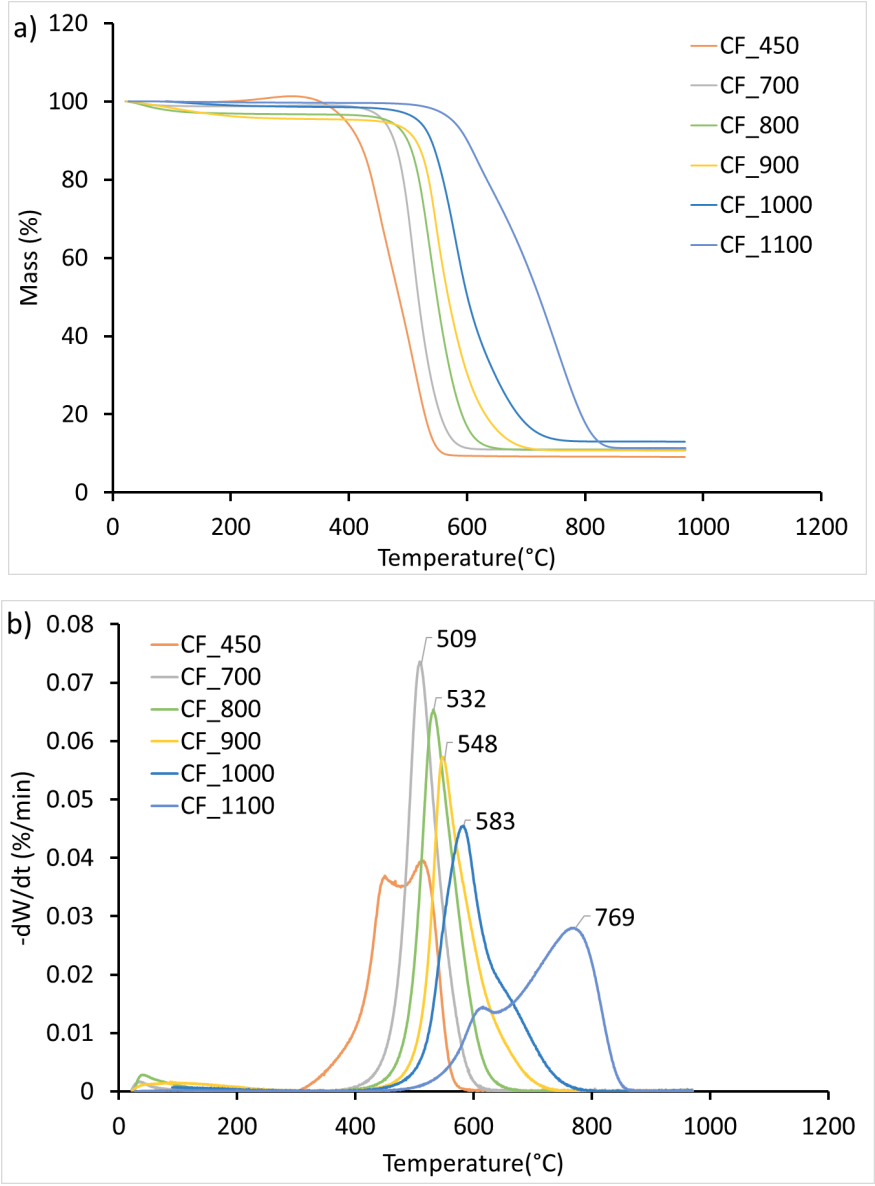

Figure 2. TGA and DTG curves for green foam (450 °C) and carbon foam treated at different temperatures (700 °C, 800 °C, 900 °C,1000 °C, 1100 °C)

Isoconversional analyses using Friedman method were conducted to evaluate oxidation kinetics of the carbon foam materials [4]. The degree of degradation (conversion, α) was estimated using the following expression:

$$\alpha = \frac{w_i - w}{w_i - w_f} \quad (1)$$

Where w_i is the initial weight of the specimen, w is the weight of the specimen at any time, w_f is the final weight of the specimen. For dynamic non-isothermal TGA with constant heating rate (β), Friedman model can be expressed by the following equation [4]:

$$ln\left(\beta \frac{d\alpha}{dT}\right)_{\alpha,i} = ln\left(Af(\alpha)\right) - \frac{E}{RT_{\alpha,i}} \quad (2)$$

Where β is the heating rate (5 °C/min, 10 °C/min, 15 °C/min, 20 °C/min), T is the temperature, $f(\alpha)$ represents dependence on extent of conversion (reaction model), E is the activation energy, R is the universal gas constant (8.3145 J/mol.K). Activation energy values estimated using the Friedman method are shown in Figure 3. Below 0.4 conversion, the green foam possessed higher activation energy values in comparison to treated foams. Above 0.4 conversion, only the 1100 °C foam activation energy values were higher than the green foam. An overall decreasing trend was noticed for foams treated at 700 °C and 800 °C. A decreasing trend followed by an increase was noticed for the 900 °C, 1000 °C, and 1100 °C foams. The minimum activation energy for these foams was at different degrees of conversion and increasing the treatment temperatures shift the minimum value toward lower conversions.

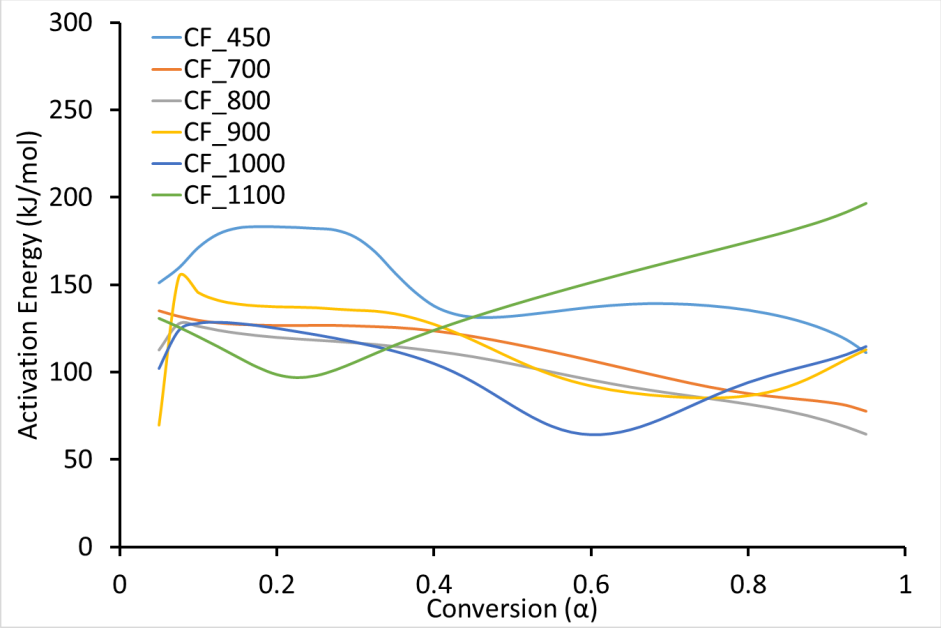

Figure 3. Activation energy at different degradation levels for green foam (450 °C) and carbon foam treated at different temperatures (700 °C, 800 °C, 900 °C,1000 °C, 1100 °C)

2.1.3. Rate of Burning

The rate of burning test outlined in ASTM D635 was used to compare the burning properties of the carbon foam material with traditional fiber cement (FC) siding product [5]. Carbon foam and James Hardie HardiePlank FC board were cut into 125 mm long by 13 mm wide test specimens. Figure 4a shows the FC samples immediately after the removal of the test flame, and Figure 4b shows the carbon foam sample during exposure to the test flame. Both materials exhibited similar burning behavior. Neither material continued to burn after the removal of the test flame, and the flame front did not reach the 25 mm reference mark. Both materials radiated red when exposed to the test flame but extinguished within five

seconds upon removal of the flame. It is worth noting the FC specimens delaminated when exposed to the test flame as shown in Figure 4a.

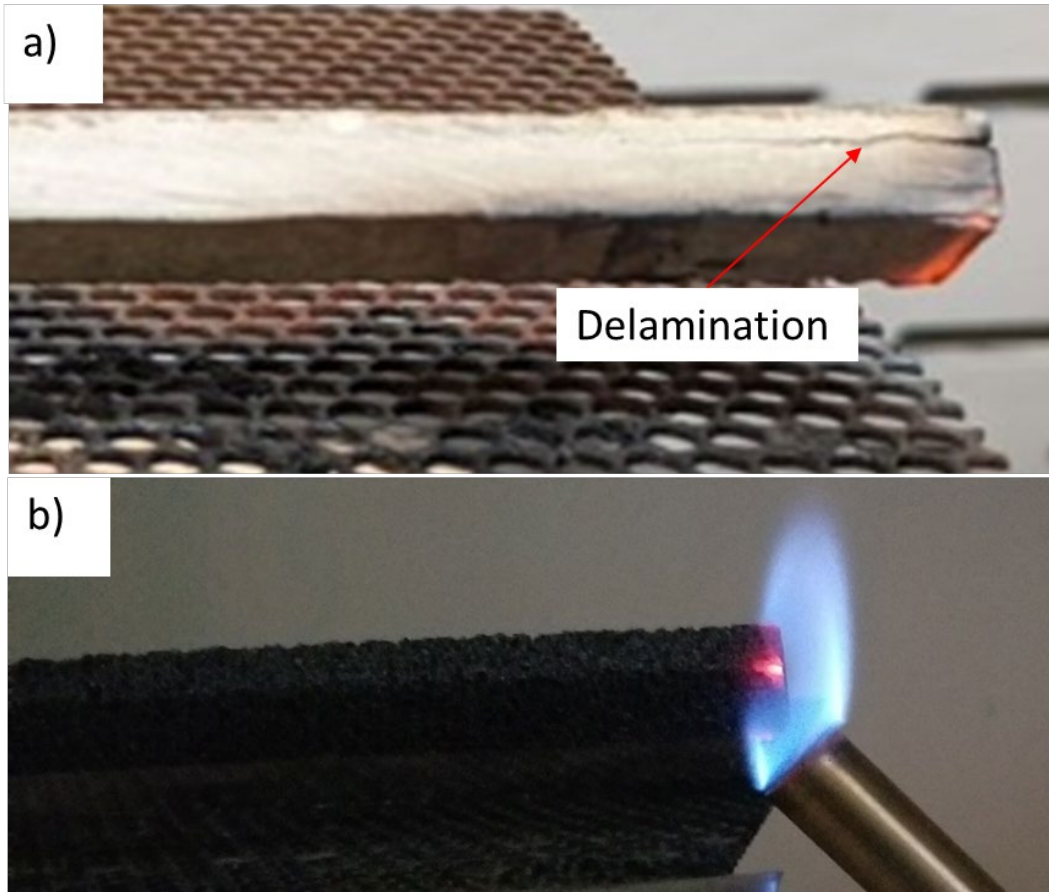

Figure 4. a) fiber cement (FC) board did not continue to burn after exposure to the flame, b) carbon foam illuminated red when exposed to the test flame but did not continue to burn after removal of the flame.

2.1.4. Density and Microstructure

The density for the carbon foam (green and treated at different temperatures) was determined using the water displacement method. As depicted in Figure 5, the density of foam increased from 32 to 37 lb/ft^3 when the material was treated at 700 °C. The density remained the same (37 lb/ft^3) for the foam treated at 800 °C, while direct proportionally with treatment temperature was observed at the higher treatment temperature range (900-1100 °C).

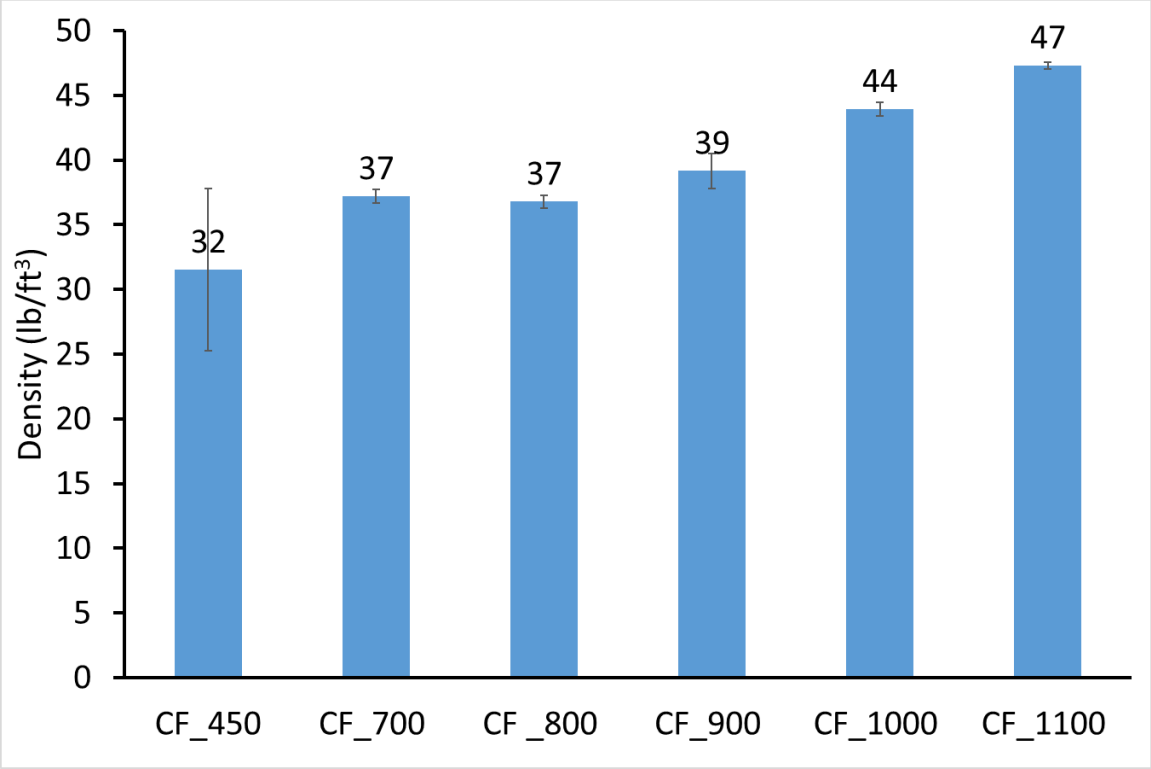

Figure 5. Density of green foam (450 °C) and carbon foam treated at different temperatures (700 °C, 800 °C, 900 °C, 1000 °C, and 1100 °C)

Micro-computed tomography (µCT) was used to investigate the foam microstructure. The µCT scans were visualized and analyzed using Avizo commercial software. Equivalent diameter and sphericity of each pore, and total porosity volume fraction were estimated for three different types of foam (green, 700 °C, 900 °C). Figure 6 depicts the 3D CT scans for foam materials at different temperatures. The porosity volume fraction for the green foam was approximately 27%. Treating the green foam at 700 °C has shown to increase the porosity level to 38.8%. Such increase can be explained as the material is still foaming and forming extra pores in the foam structure. Further increase in the treatment temperature (i.e., 900 °C) has shown to slightly decrease the porosity level to 35.7%, indicating a potential overall shrinkage of the foam. Analyses of the commercial foam indicated that the porosity volume fraction was19% for foam treated at 1100 °C. It is worth noting regardless of the porosity volume fraction, the overall volume of the foam has inverse proportionally with the treatment temperature. For example, the overall volume for green foam decreased by 17 % and 28.8% as the treatment temperature increased to 700 °C and 900 °C, respectively.

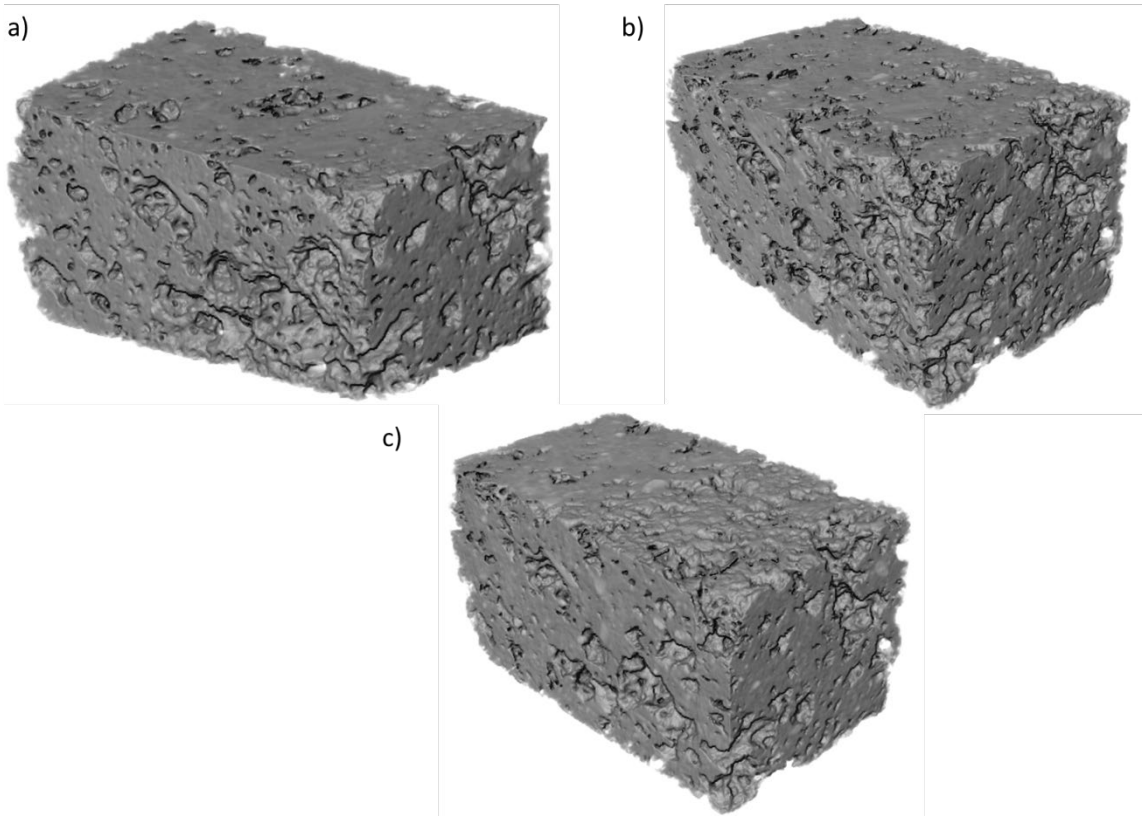

Figure 6. 3D CT scans showing a) green foam (450 °C), b) foam treated at 700 °C, and c) foam treated at 900 °C.

2.1.5. Water Absorption

Water absorption for carbon foam materials and commercial siding products was determined in accordance with ASTM C1185 [6]. Rectangular specimens (100x100 mm) were dried to a constant weight in a convection oven and then submerged in clean water for two days at room temperature. Three different types of carbon foam with different densities (20, 27, and 35 lb/ft^3) were tested and compared with James Hardie HardiePlank FC siding as shown in Figure 7. Water absorption decreased approximately 63% as the foam density increased from 20-35 lb/ft^3, while CF35 possessed a comparable water absorption level as compared to HardiePlank siding. The reduction in water absorption with density increase can be explained as less water gets trapped in the foam structure leading to lower water absorption values.

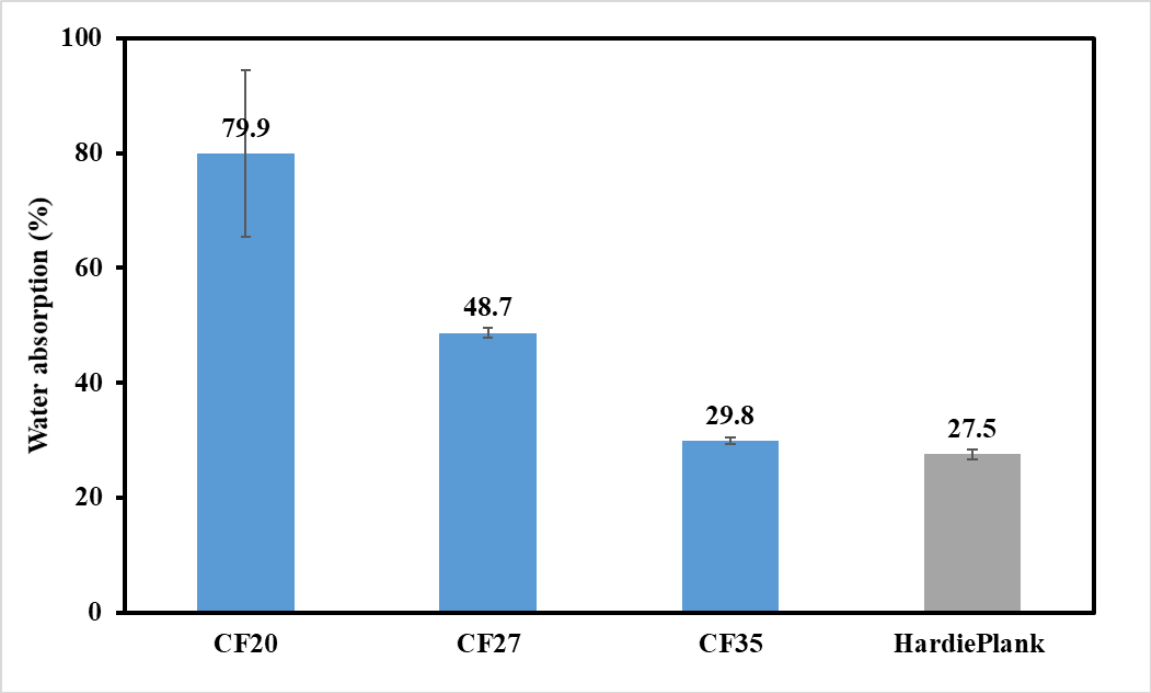

Figure 7. Water absorption for carbon foam in comparison to HardiePlank FC siding

2.1.6. Electrical Conductivity

The electrical resistivity for the carbon foam was determined using the 4-point method. Figure 8 shows electrical resistivity values for carbon foam treated at different temperatures (700, 800, 900, 1000, and 1100 °C) in comparison to commercial carbon foam. Below 700 ºC, neither the carbon foam developed in the lab nor the commercial carbon foam was conductive. At the onset of conductivity (700 °C treatment temperature), carbon foam developed in the lab has shown lower resistivity values (0.61 Ω.cm) as compared to the commercial foam (1.43 Ω.cm). The difference in the resistivity values might be attributed to 1) the difference in the coal composition, and 2) the difference in foam density. A significant drop in the resistivity values occurred at 800 ºC treatment temperature followed by a slower decreasing trend as treatment temperature increased up to 1100 ºC. At 1100 ºC, both types of foam showed identical resistivity values (0.03 Ω.cm).

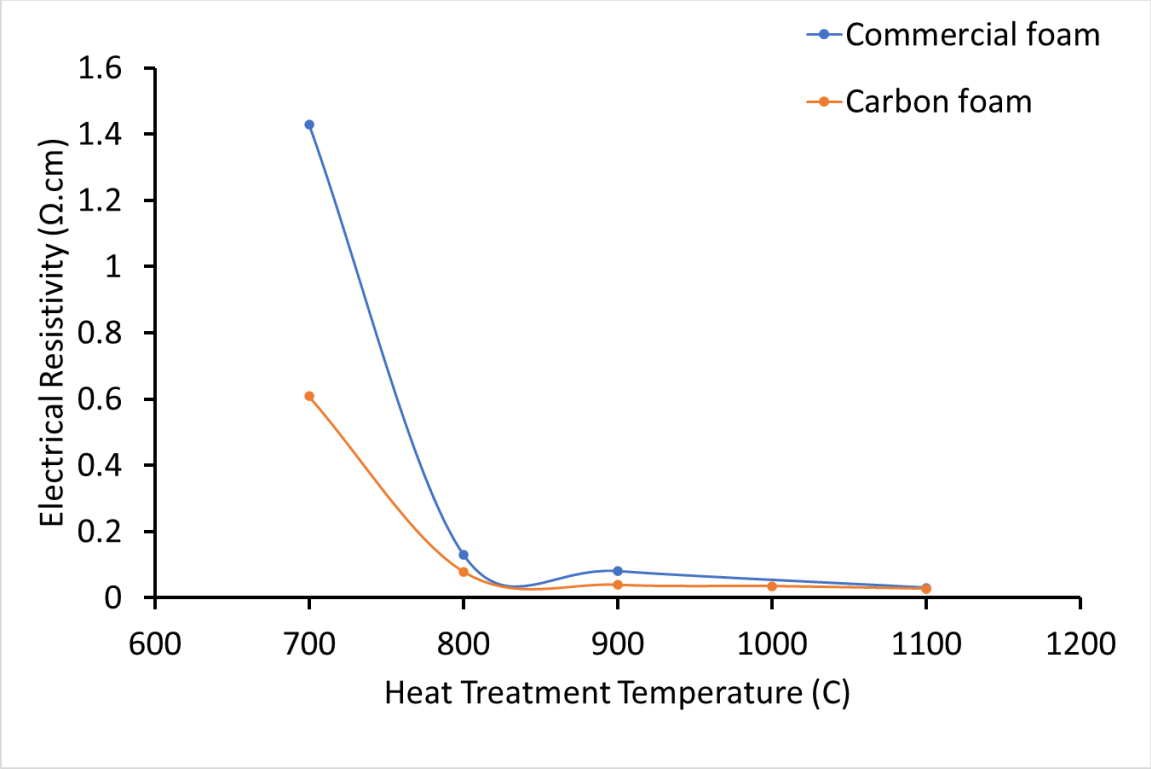

Figure 8. Electrical resistivity for treated carbon foam in comparison to commercial carbon foam

2.1.7. Flexural Properties

For usage in siding applications comparable to flat fiber cement (FC) sheets, carbon foam sheets must meet the specification of flexural strength outlined in ASTM C1186 [7]. Type A sheets must meet the flexural strength requirements under both wet and equilibrium conditions, while Type B sheets are only required to meet the standard of equilibrium testing [7]. Four grades of siding material are specified based on the flexural strength. The lowest acceptable grade, Grade I, must have a flexural strength of 4 MPa [7].

Flexural testing was performed on carbon foam and James Hardie HardiePlank FC boards as per ASTM C1185 [6]. The carbon foam materials are designated by their abbreviated names which represent the respective bulk density (lb/ft^3) as reported by CFOAM [8]. The Span-to-thickness ratio of 18 was used in the three-point bending tests with a constant displacement rate being applied at midspan. All testing was performed using an Instron 5966 universal testing machine.

Figure 9 shows the flexural strength of the carbon foam and FC materials. Equilibrium testing is shown by the blue bars. The CF20 foam achieved a flexural strength of 1.7 ± 0.5 MPa which fails to meet the lowest grade of siding. CF27 and CF35 achieved flexural strengths of 4.2 ± 0.4 MPa and 5.0 ± 0.8 MPa respectively. Both carbon foams exceed the Grade I sheet requirement for equilibrium flexural strength. The FC achieved an equilibrium flexural strength of 16.6 ± 1.5 MPa which meets the ASTM requirement for Grade III sheets. Supplemental flexural testing was performed at an elevated temperature of 100 °C. At the elevated temperature CF20, CF27, and CF35 achieved flexural strengths of 1.9 ± 0.1 MPa, 3.7 ± 0.7 MPa, and 4.5 ± 0.7 MPa respectively. At a confidence interval of 95%, the flexural strength of CF20 and CF35 at the elevated temperature proved to not be significantly different from the flexural strength at

the equilibrium temperature. At the elevated temperature, the FC exhibited a drastic decrease in flexural strength by approximately 32%.

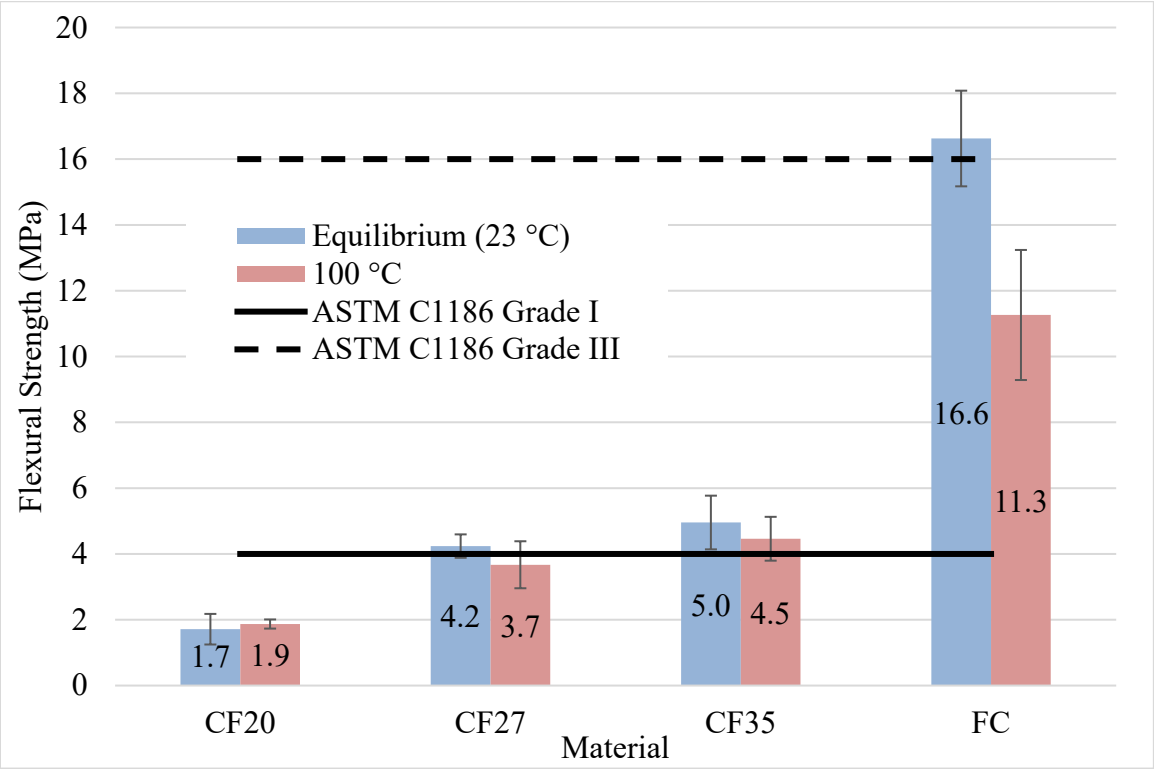

Figure 9. The carbon foam and FC flexural strengths. Error bars represent one sample standard deviation.

The flexural testing at the equilibrium and elevated temperatures was used to estimate the flexural modulus of the siding materials. The modulus was calculated following the procedure outlined in ASTM C1185 [6]. The slope of the load-displacement curve was estimated using a linear regression with an R^2 value greater than 0.99. The resulting moduli for the carbon foam and FC materials are provided in Figure 10. At the equilibrium temperature, CF20, CF27, and CF35 respectively had moduli of 0.61 ± 0.15 GPa, 0.99 ± 0.12 GPa, and 1.38 ± 0.22 GPa. As the bulk density of the foam increased, the stiffness of the carbon foam increased. The FC exhibited a modulus of 6.59 ± 0.51 GPa at room temperature. At 100 °C, CF20, CF27, and CF35 had flexural moduli of 0.73 ± 0.10 GPa, 1.36 ± 0.14 GPa, and 1.66 ± 0.23 GPa respectively. Compared to equilibrium temperature results, the three carbon foam materials had a significant increase in the modulus when compared at a confidence interval of 95%. The carbon foams exhibited a similar trend to the equilibrium testing where the material's stiffness increased with the foam's bulk density. The FC had a flexural modulus of 6.49 ± 0.66 GPa at 100 °C which was not statistically different than the modulus at the equilibrium temperature. In conclusion, both flexural strength and flexural modulus increased with the density, and carbon foams (CF27 and CF 35) met the ASTM requirements for siding application.

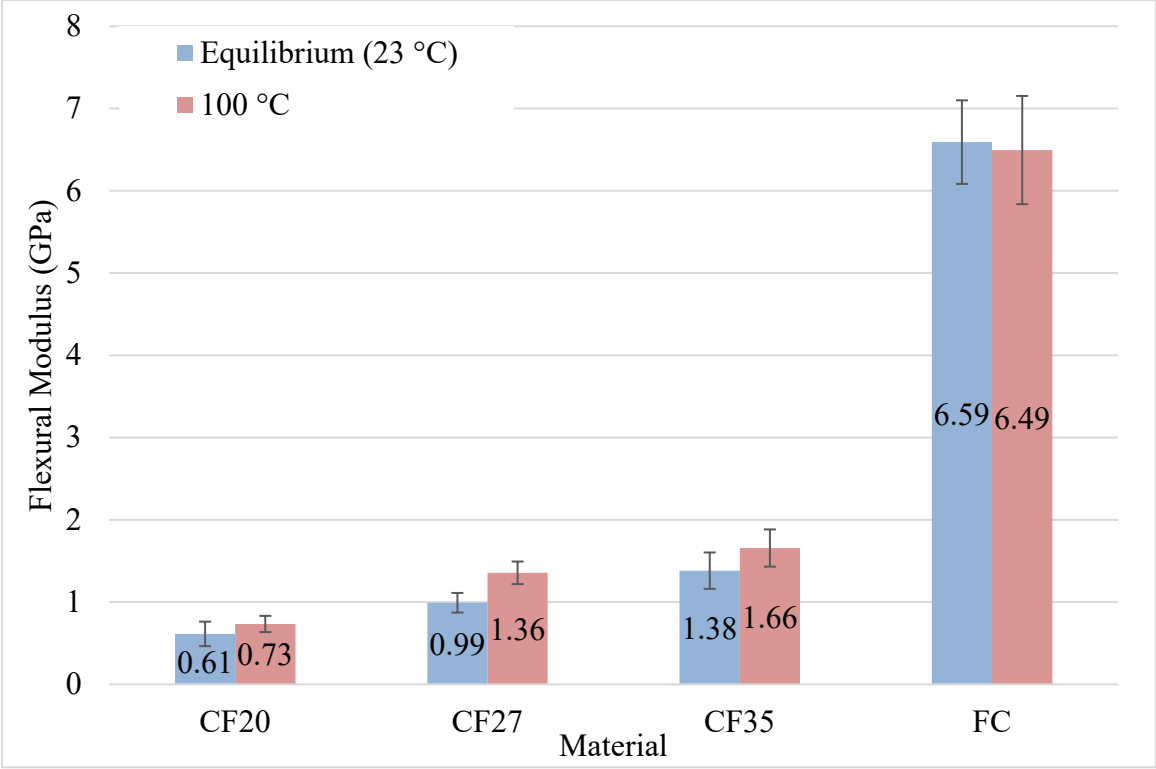

Figure 10. The flexural modulus of the commercial coal-derived carbon foam and FC materials. Error bars represent one sample standard deviation.

The effect of fiber backing sheets and plastic coating was investigated. Carbon fiber composite, glass fiber composite, and epoxy were applied on the outer side of carbon foam samples. A single sheet was adhered to the outer surface and cured in a convection oven as per recommendations by the manufacturer. The carbon foam materials are designated by their abbreviated names which represent the respective bulk density (lb/ft^3) as reported by CFOAM [8]. Flexural testing was performed on carbon foam materials as per ASTM C1185 [6]. Tests were conducted using an Instron 5966 universal testing machine. Span-to-thickness ratio was kept at 18 and all testing was performed under the same displacement rate. For usage in siding applications, carbon foam materials must meet the specification of flexural strength described in ASTM C1186 [7].

Figure 11 shows the flexural strength of the different carbon foam materials in comparison to ASTM requirements. Flexural strength for CF20 with no fiber backing or plastic coating (CF20 plain) was below the ASTM requirement for Grad I materials. At higher densities, carbon foams (CF27 and CF35) have met the ASTM requirements. Applying the plastic coating has shown to significantly increase the flexural strength of all types of foam with the biggest impact being on the lower density foam (i.e., CF20) as the flexural strength increased by almost 205%. Both the carbon fiber and glass fiber coated foams possessed substantially improved flexural strength with CF27 and CF 35 exceeding the ASTM requirement for Grade III materials. Similar to plastic coating, flexural strength for the carbon foams with carbon and glass fiber increased with foam density with the carbon fiber composite possessing higher strength values. Figure 12 shows carbon foam samples with glass and carbon fiber backing materials after being tested.

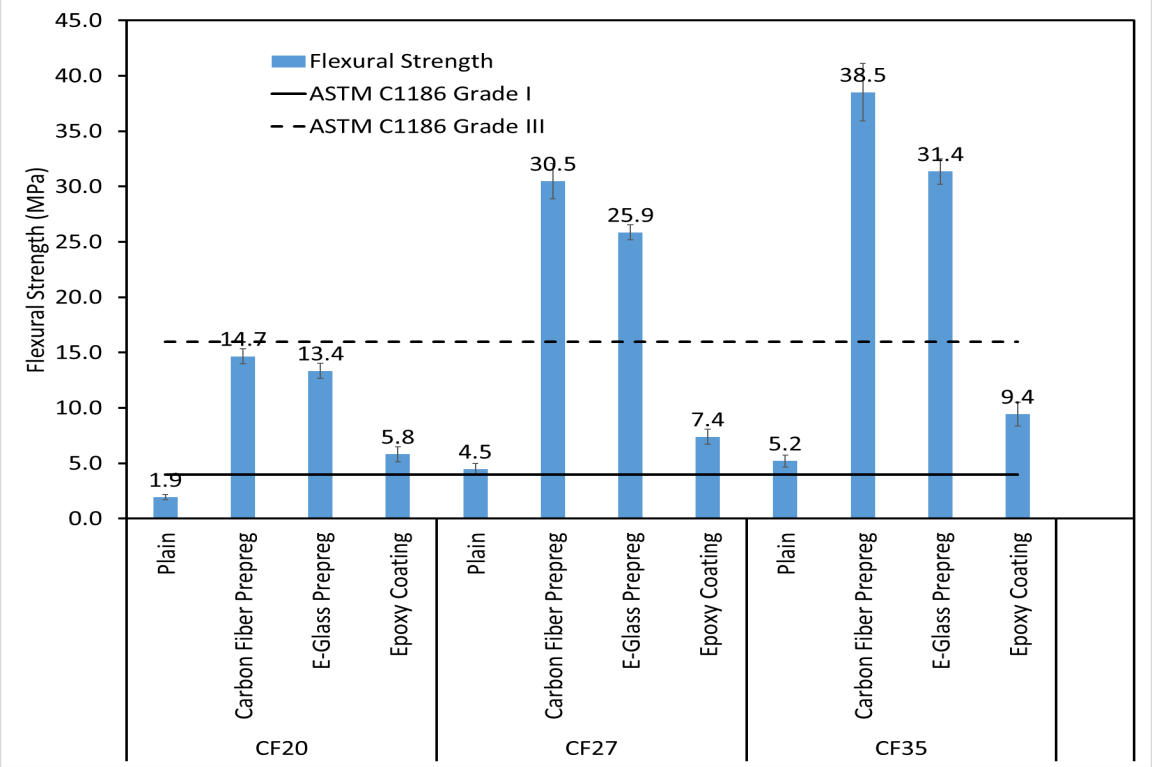

Figure 11: Flexural Strength for coal-derived carbon foam materials with and without fiber backing. Error bars represent one sample standard deviation

Figure 12: Carbon foam materials with fiberglass (right) and carbon fiber (left) after flexural testing

2.1.8. Molecular Dynamic Simulation of Coal Siding Materials

A clear understanding of the basic structure of coal is pivotal to understanding the formation of carbon foam during extrusion in a suitable temperature window. There are significant changes in the structure and in the carbon bonding environment when the coal transforms into a carbon foam when treated at 420°C. To gain an insight into these phenomena, we started with the simple hand-drawn model proposed by Solomon [9]. We believe that the elemental composition of high-rank coal used for the foam extrusion is similar to this model. The model was relaxed using conjugate gradient and then equilibrated at 300K using Vienna ab-initio Simulation Package (VASP) [10] to allow for structural relaxation to find a suitable energy minimum configuration. This reduced the energy of the configuration, and the system is now ready for further elevated temperature simulations. The relaxed 3-D model is shown in Figure 13. We were also working on the maceral vitrinite and especially exploring the role of phenyl groups in the foaming process.

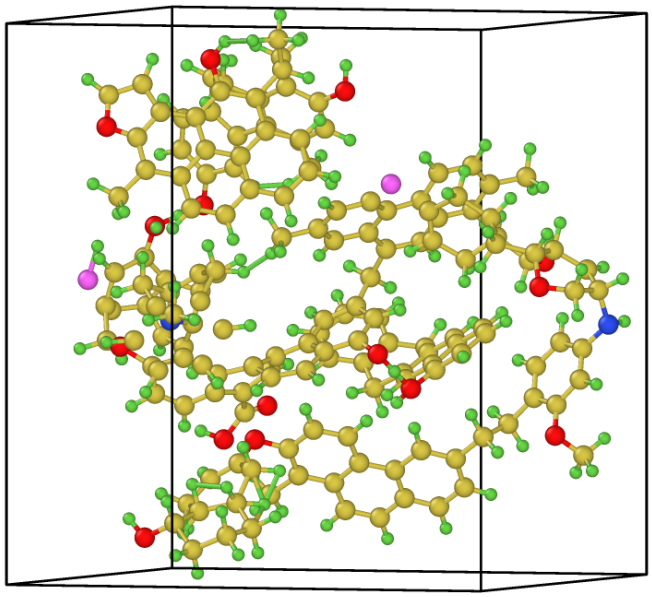

Figure 13; 3-D model of coal generated derived from Solomon's mode [9]. Yellow, green, red, blue, and pink atoms represent carbon, hydrogen, oxygen, nitrogen, and sulfur, respectively

Molecular Dynamics simulation of Graphitization of a-C using Machine-Learning

We simulated the process of graphitization of amorphous carbon over a wide range of densities, temperatures, and system sizes. Multiple simulations were done to determine the transition temperature while the simulations with different system sizes were carried out to analyze the size effects and the periodic boundary conditions on the graphitization process. The calculations were performed with DFT the code VASP (Vienna ab initio Simulation Package). The atomistic models of amorphous carbon at different densities were taken through ab initio simulation at different temperatures with the temperature controlled by a Nose' thermostat. The simulation time varied between 100-120 ps, extended from the previous study with 40 ps, to let the system explore a larger configurational space and allow for a thorough analysis of stability. In this report, we present the details of the calculations obtained for graphitization of a-C at a density of 2440 kg/m^3. The calculations were repeated on two different models, labelled M-1 and M-2, both with 160 atoms. Figure 14 suggests that there is onset of graphitization at

about 2700K in both the models. However, there is a significant increase in the sp^2 fraction even at 2500K although not much clear layering is seen.

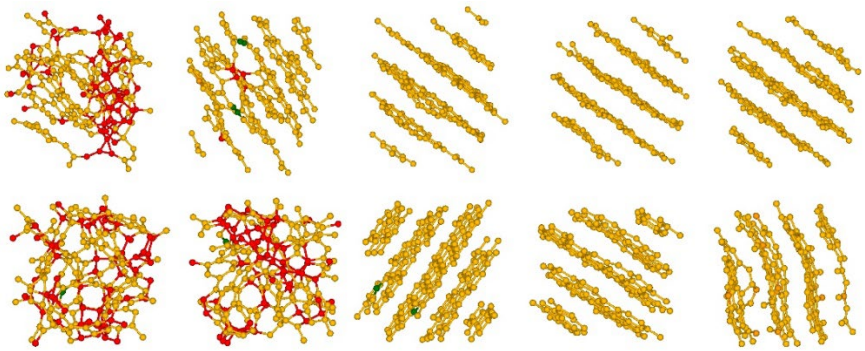

Figure 14: Comparison of the energy relaxed structure of M-1 (top) and M-2 (bottom) at room temperature (left most) with the structure after constant temperature simulation at different temperatures (2500K, 2700K, 3000K, 3300K). Structures at 3300K are on the extreme right. The planes consist of layers of amorphous graphene (see Fig. 15).

We have made considerable progress on understanding the electronic origins of the layers and show that dispersive Van der Waals interactions are not necessary to induce and stabilize layering, contrary to much conventional wisdom. We checked this in detail by repeating these simulations with Van der Waals corrections included and it made no qualitative difference in the layering process or the structure of the atomic layers themselves. In Figure 15 we show one amorphous graphene plane: the carbon atoms are all sp^2, but note the ring disorder (pentagons, hexagons and heptagons) in interesting contrast to perfectly hexagonal graphene/graphite. We have named this material *amorphous graphite* (a-G) [11].

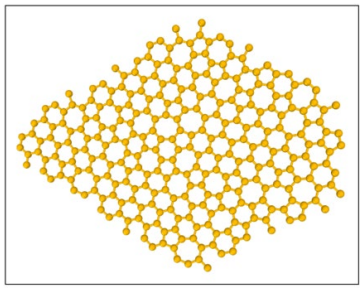

Figure 15: A representative layer of the a-G solid. Note the odd-membered rings.

Using a Machine learning potential GAP [12], we have also simulated larger system (~1000 atoms) to study the effects of finite size and to get better understanding of a-G. This development gives us the opportunity to study many other properties (vibrational, thermal, electrical, mechanical). We illustrate one such model in Figure 16.

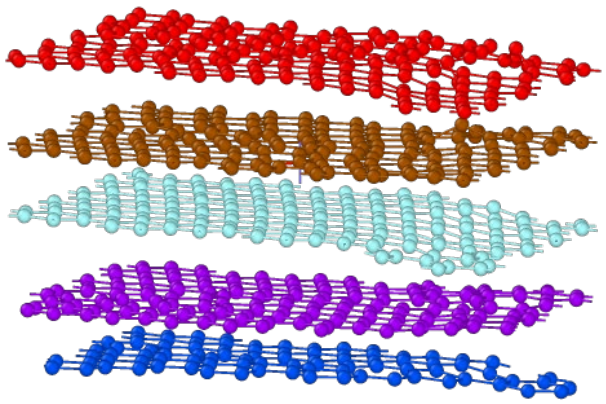

Figure 16: Amorphous graphite (a-G) with 1000 atoms. A perfect graphene plane can be seen in the middle layer

3. Coal-Enhanced Fiber Cement Composites

Fiber cement composites utilizing carbon foam particles as aggregate sought to reduce the density of the siding material while maintaining comparable mechanical and physical properties to traditionally used fillers. A control formulation utilizing silica sand as the filler material was developed based on weight fractions from literature [13], [14]. The control formulation used 50 wt.% sand filler. The carbon foam-based composites were then developed at the constant volume fractions of the control composite. Table 1 shows the weight and volume fractions of the fiber cement composites. Production of fiber cementitious samples at the lab scale utilized a simulated batch-wise Hatschek process. Mastercraft Type I Portland cement was used as the base for the fiber cement composites. Cascade Pacific Grade 670 unbleached Kraft softwood pulp was blended with water to fibrillate the material for introduction during the mixing process [15]. Buddy Rhodes 6 mm 5 denier polyvinyl alcohol (PVA) fibers were used to improve the toughness of the composite matrix [16]. Control samples were developed using Quikrete Premium Play Sand as the aggregate filler material, and samples were created using green carbon foam (GCF) and calcined carbon foam (CCF) millings from CFOAM LLC. The GCF and CCF were sieved to between 210 and 595 microns. The millings were from CF30 production. Additionally, all formulations included the addition of 0.1 wt.% ADVA Cast 575 superplasticizer to act as a surfactant for improved filler wetting and workability of the matrix [17]. The sheets were air cured at room temperature for 6- and 28-day periods. The composite sheets developed are shown in Figure 17. The sheets were cut using a diamond bladed saw into rectangular test samples.

Table 1. The fiber cement composite formulations investigated with constant volume fractions based on the control sand formulation.

		Weight Fractions (wt. %)	Volume Fractions (vol. %)
Control Sand	Portland Cement	41.5	42.8
	Softwood Pulp	8.0	18.5
	PVA Fibers	0.5	0.5
	Sand Filler	50.0	38.2
GCF	Portland Cement	57.1	42.8
	Softwood Pulp	11.0	18.5
	PVA Fibers	0.7	0.5
	GCF Filler	31.2	38.2
CCF	Portland Cement	52.2	42.8
	Softwood Pulp	10.1	18.5

PVA Fibers	0.6	0.5
CCF Filler	37.1	38.2

Figure 17: The control sand (left), GCF (middle), and CCF (right) fiber cement composite sheets during the curing process.

The microstructure of the carbon foam enhanced fiber cement was compared to the microstructure of the traditional sand filled fiber cement composite. The 28-day silica sand, GCF, and CCF composite samples were investigated using a Leica DVM6 optical microscope. Wet-polished cross-sections were prepared to better show cement-aggregate boundaries, and images were generated at 200x magnification before being digitally stitched. The microscopy images are shown in Figure 18. When comparing the composite microstructures, all three cement composites show adequate particle dispersion throughout the cross-section. Additionally, the interfacial boundary between the cement matrix and the filler material does not show signs of large porosity in neither the sand nor the carbon foam composites. One noticeable difference between the composite microstructures is in the particle shape. As shown in Figure 18, the GCF and CCF particles exhibit more angular shapes and sharp points compared to the rounder sand particles.

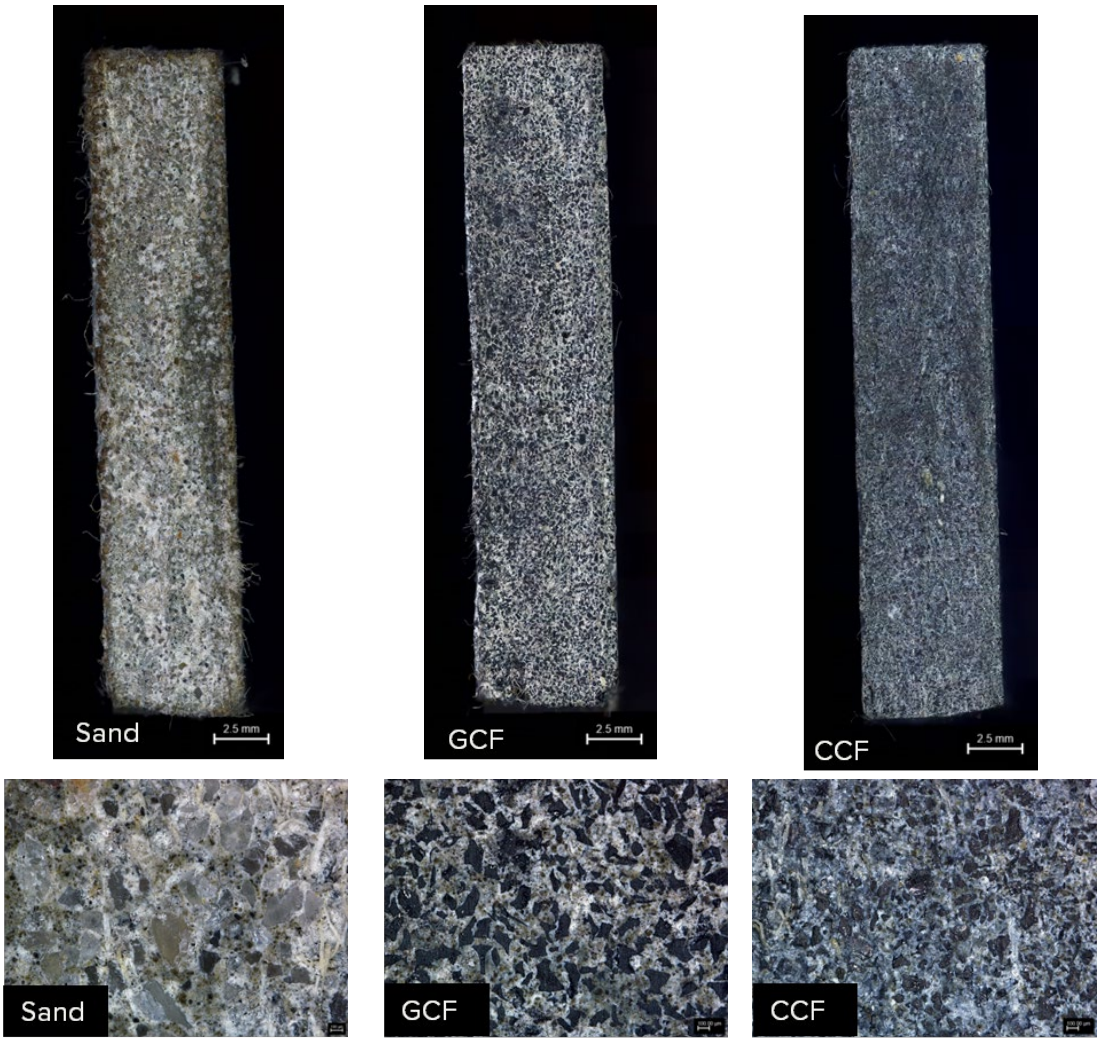

Figure 18: The optical microscopy of the sand, GCF, and CCF cement composites.

The mechanical and physical properties of the fiber cement composites were evaluated in correspondence with ASTM C1185 and ASTM C1186 [6], [7]. All properties were evaluated after a 6-day and 28-day curing period. For fiber cementitious materials to be used in exterior applications exposed to direct rain or snow, the material must meet the Type A flexural strength requirements. The sheet is tested in both a dry, equilibrium (EQ) condition and in a saturated, wet condition. Figure 19 shows the results of the EQ and wet flexural testing of the cement composites. After the 28-day cure period, the sand, GCF, and CCF filled composites meet the 4 MPa flexural strength requirement for Grade I siding in both the EQ and wet

conditions. At a 95% level of confidence, the 28-day EQ and wet flexural strengths of the carbon composites are not statistically different than the flexural strengths of the sand filled composite.

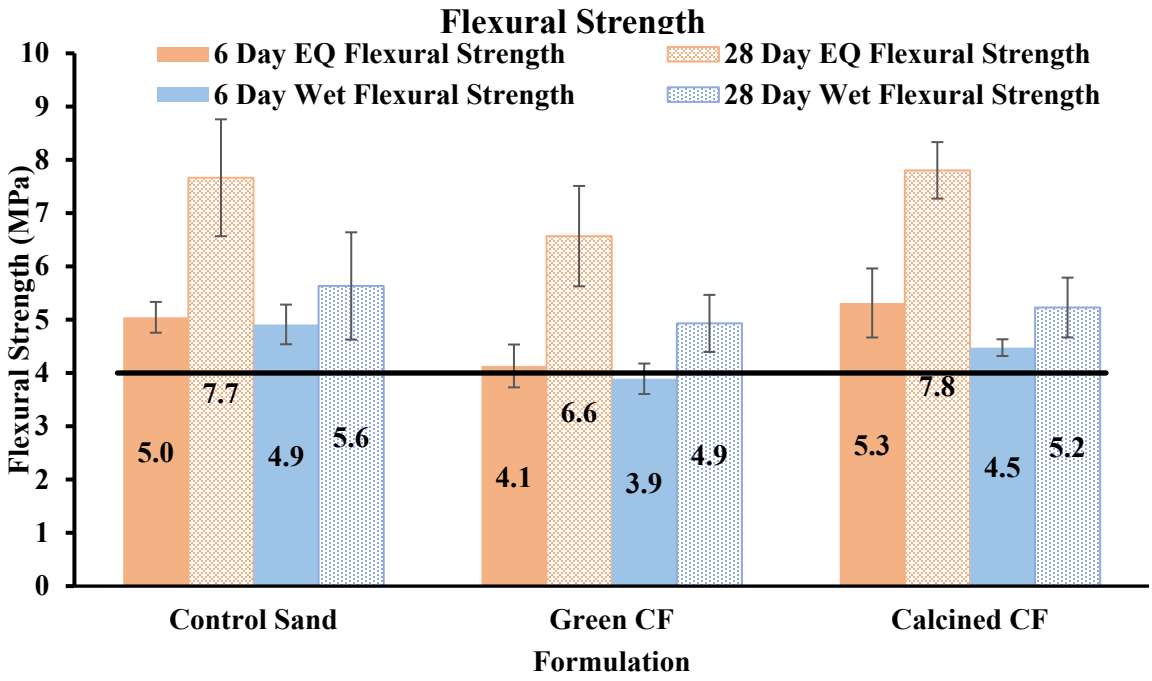

Figure 19: The 6-day and 28-day EQ and wet flexural strength of the fiber cement composites.

Figure 20 illustrates the reduction in the composite density due to the light-weight carbon filler. In comparison to the sand filled composite, the GCF composite exhibits a 29.3 % weight saving and the CCF composite exhibits a 14.9 % weight saving. The reduction in material density seeks to improve the material handling during transport and installation.

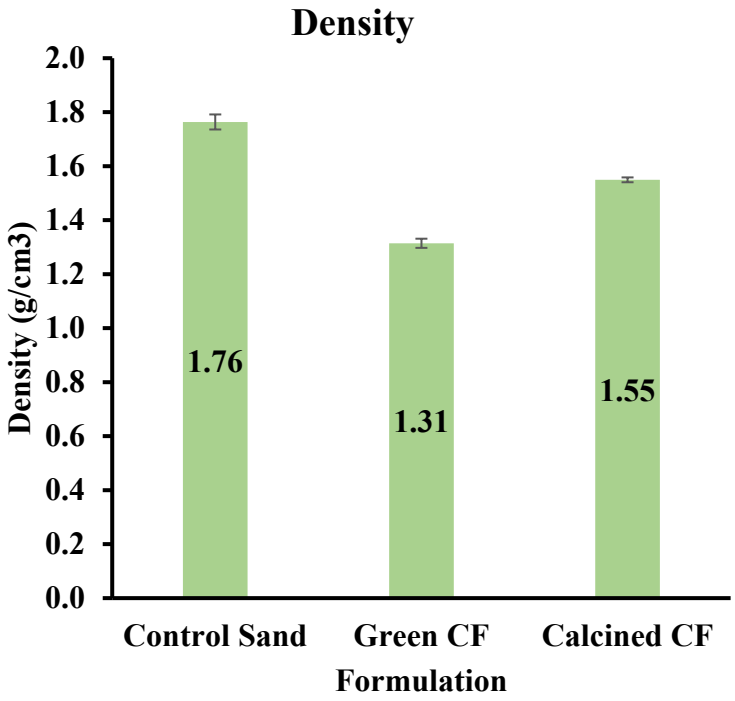

Figure 20: The carbon foam filler reduced the matrix density compared to the traditional sand filler.

Figure 21 and Figure 22 present the moisture content and water absorption results, respectively, for the composite formulations. The GCF composites exhibited greater moisture content and water absorption compared to the sand and CCF composites.

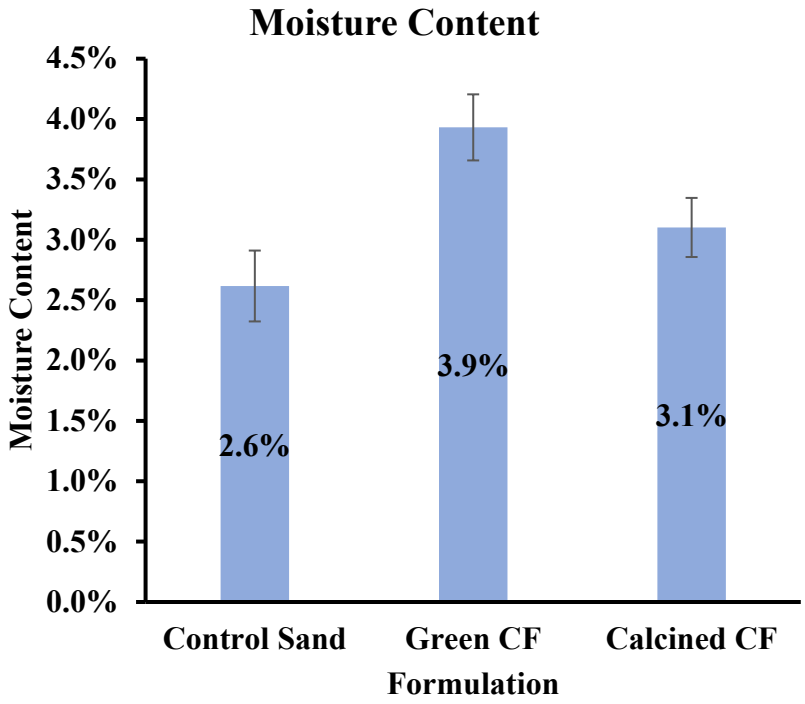

Figure 21: The moisture content of the fiber cement composites after 28 days.

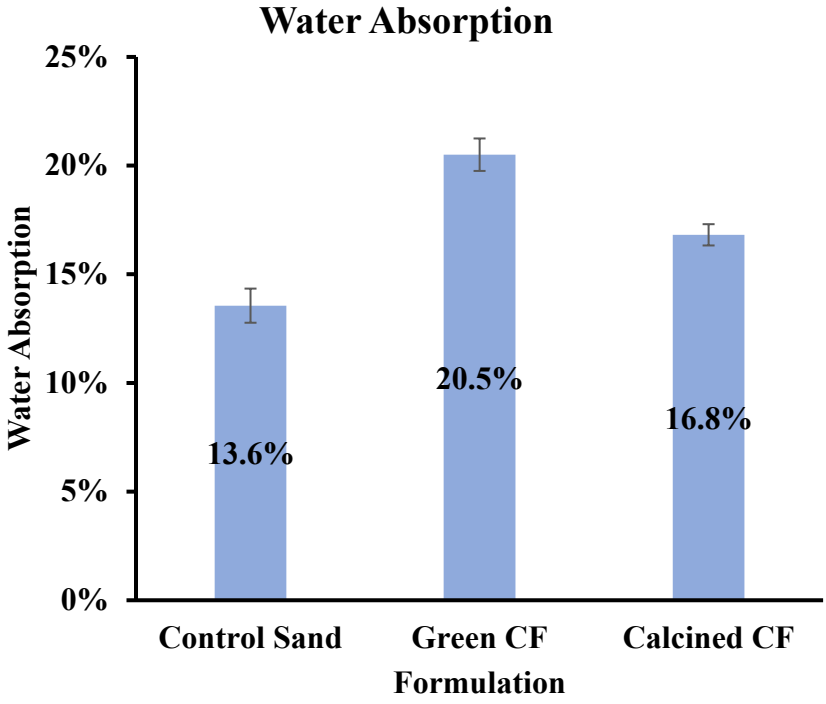

Figure 22: The water absorption of the fiber cement composites.

The cement composites were tested for flammability using the ASTM D635 Rate of Burning test as a lab scaled assessment of the material [5]. Figure 23 shows the samples during the rate of burning tests. All three formulations failed to ignite during the test, and the flame front did not reach the 25 mm reference mark.

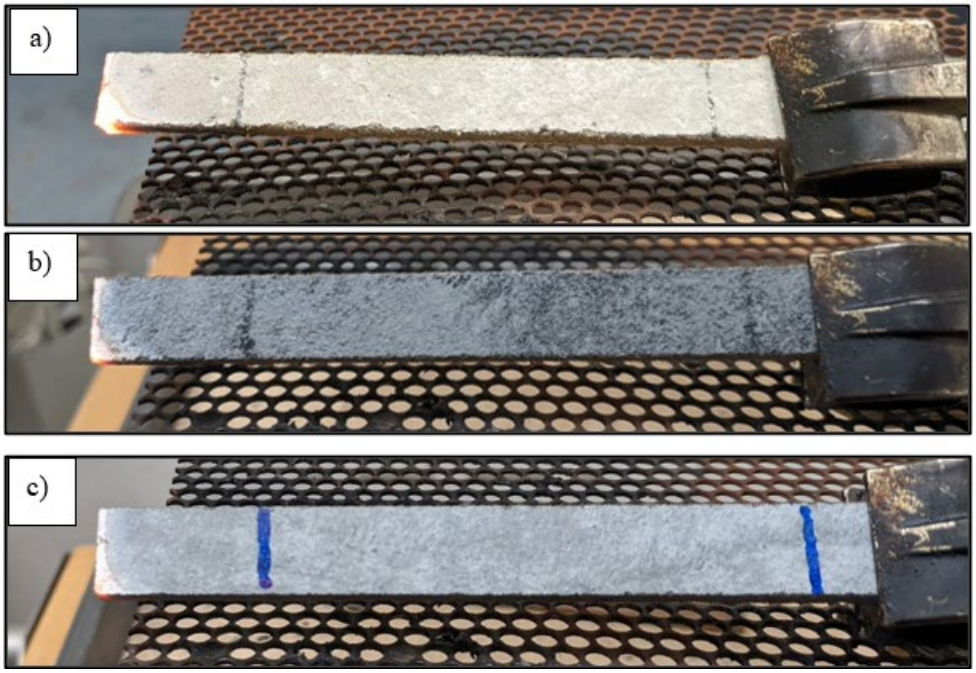

Figure 23: The three formulations during the rate of burning test immediately after the removal of the test flame. a) control sand composite, b) GCF composite, c) CCF composite.

Fiber cement composites were also investigated for high carbon loading content. A 70 wt.% carbon formulation was developed as shown in Table 2. Chopped carbon fibers (¼" long) are sourced from Fibre Glast Developments Corp [18]. The composites are mixed with 0.2 wt.% ADVA Cast 575 to improve the workability with the high filler content. The composites are air cured prior to testing. The experimental composite sheet is shown in Figure 24.

Table 2. The 70 wt.% carbon fiber cement formulation.

		Weight Fractions (wt. %)
Control Sand	Portland Cement	30.0
	¼" Chopped Carbon Fibers	1.0
	CCF Filler	69.0

Figure 24: The 70 wt.% carbon fiber cement composite sheet.

The flexural strength of the 70 wt.% carbon composites is shown in Figure 25, and the density, moisture content, and water absorption of the 70 wt.% carbon composites are shown in

Table 3. The 70 wt.% carbon composite meets the ASTM required strength in the EQ condition after the 28-day curing period but fails to meet the strength requirement in the wet condition.

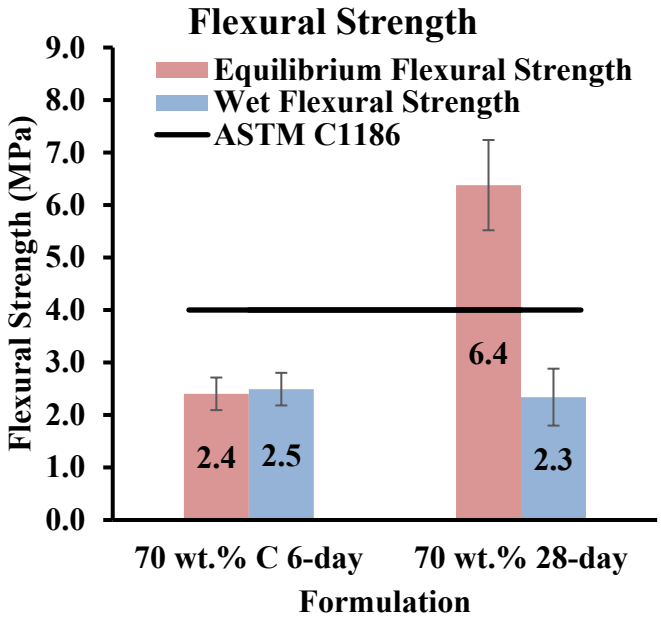

Figure 25: The 6-day and 28-day flexural strength of the 70 wt.% carbon composites.

Table 3. Density, moisture content, and water absorption of 70 wt.% carbon fiber cement composites.

70 wt.% Carbon	Density (g/cm^3)	Moisture Content (%)	Water Absorption (%)
6-day	1.23	3.23	30.16
28-day	1.07	5.49	24.63

4. Techno-economic and Lifecycle Analyses

4.1. Overview

Techno-economic analyses were conducted for a new coal foam siding manufacturing plant. Base assumptions used in the study are listed below:

1. 25,000 lb/hr of siding product generated based on a formulation consisting of 98% coal and 2% additives.
2. Plant operates for 24 hours per day for 50 weeks per year, with an assumed capacity factor of 85%
3. Taxes and insurance are calculated at 2% each of the Capital Cost.
4. The siding density is 40 lb/ft^3 and a cross-sectional area of 0.011 ft^2.
5. The siding manufacturer's selling price yields an internal rate of return (IRR) of 30%, based on a capital cost spread over two years and profits recovered over 20 years.

The block flow diagram shown below illustrates the components and unit operations required to manufacture the coal foam siding. The coal is received via truck and dried to 1% moisture prior to foaming. The foaming process produces a green coal foam siding core. The siding core is then treated in a kiln to induce further vitrification of the foam network and cooled. Backing material is applied to the foam, sprayed with primer, and cut to the desired length (typically 12 ft). To reduce the environmental impact of the plant, the foam dust due to cutting is reclaimed.

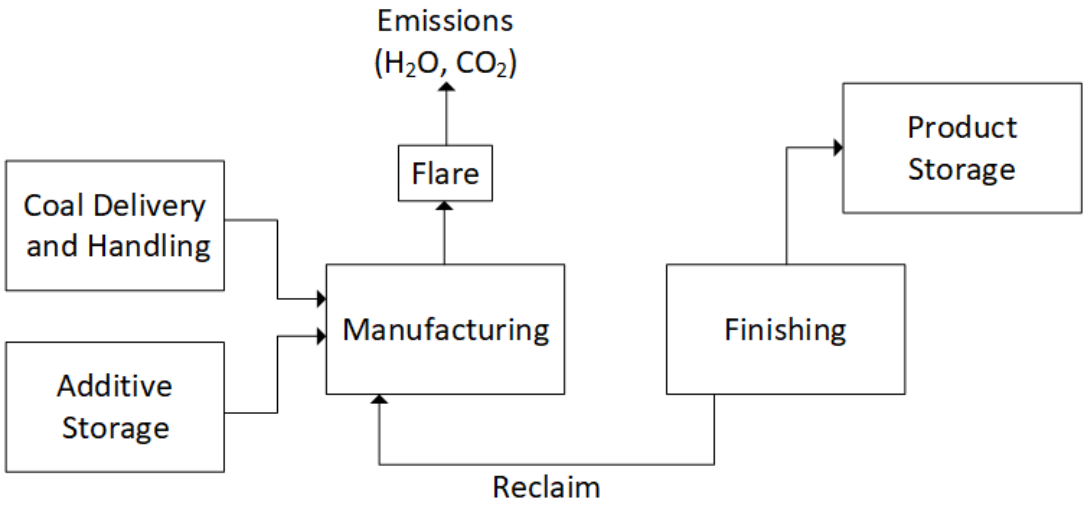

Figure 26: Block flow diagram for a proposed siding manufacturing.

4.2. Base Case Analysis

Using the base assumptions, the overall capital (includes 15% contingency) and operating costs for a new coal foam siding plant were developed. The base case financial figures are shown in Table 4.

Table 4: Carbon foam siding base case cost analysis results.

Cost	Comments	Cost
Capital Cost	*Equipment*	$199,607,000
	Building and Land	$11,434,000
Fixed OPEX	*Labor*	$18,800,000
	Maintenance and Warranties	$12,000,000
	Taxes and Insurance	$6,031,000
Variable OPEX	*Utilities*	$15,422,000
	Chemicals	$15,500,000
	Freight and Packaging	$3,000,000
Manufacturing Cost ($/linear ft)	*Excludes Capital Cost and intermediary markup*	$0.30

Conducting an internal rate of return (IRR) analysis assuming capital costs were incurred over an initial two-year period and a target of 30% return resulting in a manufacturer's sales cost of $0.60/ft. Assuming an additional 30% distribution markup, the sales cost to the end consumer is $0.78/ft. Current sales pricing for fiber cement siding is $1.02/ft, indicating the carbon foam siding material can potentially provide a greater than 20% reduction in pricing.

A previous cradle-to-gate life cycle analysis (LCA) for coal-to-products was adjusted for the coal siding process [8]. This LCA accounted for coal mining, transportation, and manufacturing (pulverization/drying, extruder, kiln, etc.). Results indicate specific emissions (SE) associated with coal siding manufacturing are 0.85 kg_{CO2}/ft^2, a >65% reduction compared to 2.5 kg_{CO2}/ft^2 for FC siding, less than stucco (1.5 kg_{CO2}/ft^2) and approaching vinyl (0.7 kg_{CO2}/ft^2) indicating the potential value of introducing coal into this building material segment. In addition, as coal siding will contain minimal silica content (only ash content of coal) offering potential health benefits for construction workers installing FC materials.

4.3. Sensitivity Analysis

The sensitivity of manufacturing cost is due to changes in product density, feedstock pricing, and manufacturing utilities. A summary of the impact of parameters on carbon foam siding costs is provided in Table 5.

Table 5: Carbon foam siding manufacturing costs sensitivity results

Parameter	Cost Sensitivity (%)
Cost of Coal (±25%)	-3.3 to +6.7
Cost of Backing (±25%)	-6.7 to +10.0
Capital Contingency (+25%)	0 to +3.3
Cost of Electricity (±20%)	-3.3 to 6.7
Foam Density (20, 30 lbs/ft^3)	+49.0 to +75.7

The sensitivity analyses indicate carbon foam density has the greatest influence on manufacturing price. Although lower-density siding manufacturing can be achieved the lower potential manufacturing price will be offset by increased backing and potential insurance. Additional parameters show a much lower impact on manufacturing costs.

4.4. Technology Gap Analysis

The project-matured carbon foam siding manufacturing to TRL 4/5 as the capability to continuously manufacture carbon foam was exhibited using bench-scale equipment and carbon foam material met ASTM C1186 flexural strength specs. Techno-economic analyses also indicate carbon foam siding materials potentially offer cost savings of 20% in comparison to current fiber cement materials.

This project provides an ideal foundation for further development of continuous carbon foam manufacturing. Further development of carbon foam siding materials will require scaling the continuous manufacturing process. The team recommends the next stage of development utilize a continuous pilot-scale manufacturing system that will allow the production of carbon foam products with commercially relevant dimensions (5/16-in by 8.25-in). Further, a continuous environmentally controlled continuous kiln should be utilized to vitrify green carbon foam into final siding core structures. Applications of backing and deposition of primer should also be investigated. Mass balances for trace components found in coal should also be analyzed to determine emissions and speciation. Prototype carbon foam siding products are to be tested according to ASTM C1186 to further evaluate performance and market compliance. Finally, existing techno-economic analyses should be updated with pilot-scale material and energy balances to further refine manufacturing costs and price competitiveness. The project team estimates the costs associated with the next stage of development will require an investment of $800 to 1,250 thousand. If successful, the next stage of development would mature the technology to TRL 7.

5. References

[1] A. A. Azni, W. A. W. A. K. Ghani, A. Idris, M. F. Z. Ja'afar, M. A. M. Salleh, and N. S. Ishak, "Microwave-assisted pyrolysis of EFB-derived biochar as potential renewable solid fuel for power generation: Biochar versus sub-bituminous coal," *Renewable Energy*, vol. 142, pp. 123–129, Nov. 2019, doi: 10.1016/j.renene.2019.04.035.

[2] S. Vyazovkin *et al.*, "ICTAC Kinetics Committee recommendations for collecting experimental thermal analysis data for kinetic computations," *Thermochimica Acta*, vol. 590, pp. 1–23, Aug. 2014, doi: 10.1016/j.tca.2014.05.036.

[3] S. Vyazovkin, A. K. Burnham, J. M. Criado, L. A. Pérez-Maqueda, C. Popescu, and N. Sbirrazzuoli, "ICTAC Kinetics Committee recommendations for performing kinetic computations on thermal analysis data," *Thermochimica Acta*, vol. 520, no. 1–2, pp. 1–19, Jun. 2011, doi: 10.1016/j.tca.2011.03.034.

[4] H. L. Friedman, "Kinetics of thermal degradation of char-forming plastics from thermogravimetry. Application to a phenolic plastic," *J. Polym. Sci. C*, vol. 6, pp. 183–195, 1964.

[5] ASTM, "ASTM D635 - 18 Standard Test Method for Rate of Burning and/or Extent and Time of Burning of Plastics in a Horizontal Position." ASTM, 2018.

[6] ASTM, "ASTM C1185 - 08 Standard Test Methods for Sampling and Testing Non-Asbestos Fiber-Cement Flat Sheet, Roofing and Siding Shingles, and Clapboards." ASTM, Nov. 2016.

[7] ASTM, "ASTM C1186 - 08 Standard Specification for Flat Fiber-Cement Sheets." ASTM, Nov. 2016.

[8] "CFOAM® Carbon Foam," *CFOAM® Carbon Foam*. https://www.cfoam.com/whatis/ (accessed Jan. 03, 2022).

[9] P. R. Solomon, T. H. Fletcher, and R. J. Pugmire, "Progress in coal pyrolysis," *Fuel*, vol. 72, no. 5, pp. 587–597, May 1993, doi: 10.1016/0016-2361(93)90570-R.

[10] G. Kresse and J. Furthmüller, "Efficient iterative schemes for *ab initio* total-energy calculations using a plane-wave basis set," *Phys. Rev. B*, vol. 54, no. 16, pp. 11169–11186, Oct. 1996, doi: 10.1103/PhysRevB.54.11169.

[11] R. Thapa, C. Ugwumadu, K. Nepal, J. Trembly, and D. Drabold, "Ab initio simulation of layered amorphous graphene," *arXiv:2202.11021 [cond-mat]*, Feb. 2022, Accessed: Apr. 25, 2022. [Online]. Available: http://arxiv.org/abs/2202.11021

[12] V. L. Deringer and G. Csányi, "Machine learning based interatomic potential for amorphous carbon," *Phys. Rev. B*, vol. 95, no. 9, p. 094203, Mar. 2017, doi: 10.1103/PhysRevB.95.094203.

[13] A. M. Soydan, A. K. Sari, B. Duymaz, R. Akdeniz, and B. Tunaboylu, "Air-Cured Fiber-Cement Composite Mixtures with Different Types of Cellulose Fibers," *Advances in Materials Science and Engineering*, vol. 2018, p. e3841514, Jan. 2018, doi: 10.1155/2018/3841514.

[14] A. M. Soydan, A. Sari, B. Duymaz, R. Akdeniz, and B. Tunaboylu, "Characterization of Fiber-Cement Composites Reinforced with Alternate Cellulosic Fibers," *Anadolu University Journal of Science and Technology A - Applied Sciences and Engineering*, vol. 19, no. 3, Art. no. 3, Sep. 2018, doi: 10.18038/aubtda.338380.

[15] Cascade Pacific Pulp LLC, "Unbleached Kraft Pulp Grade 670." Cascade Pacific Pulp LLC, 2022.

[16] Buddy Rhodes Concrete, "Buddy Rhodes PVA Fibers." [Online]. Available: https://www.smooth-on.com/tb/files/BUDDY_RHODES_PVA_FIBERS.pdf

[17] "ADVA® Cast 575 Data Sheet | GCP Applied Technologies." https://gcpat.com/en/solutions/products/adva-cast-high-range-water-reducers/adva-cast-575-data-sheet (accessed Aug. 23, 2022).

[18] Fibre Glast, "1/4" Chopped Graphite Fibers," *Fibre Glast Developments Corp*. https://www.fibreglast.com/product/14_Chopped_Graphite_Fibers_571 (accessed Jul. 12, 2022).